Journal of Solid State Chemistry **152,** 229–235 (2000)
doi:10.1006/jssc.2000.8687, available online at http://www.idealibrary.com on IDEAL®

Novel Organic–Inorganic Layered Compounds Derived from Simple Coordination Building Blocks: Synthesis and Structural Characterization of $(H_3NCH_2CH_2NH_3)[Fe(C_2O_4)MoO_4]$ and $Fe(H_2NCH_2CH_2NH_2)MoO_4$

Songping D. Huang[1] and Yongkui Shan

Department of Chemistry, Kent State University, Kent, Ohio 44242

Two new hybrid organic–inorganic compounds $(H_3NCH_2CH_2NH_3)[Fe(C_2O_4)MoO_4]$ (1) and $Fe(H_2NCH_2CH_2NH_2)$ (2) were synthesized by the hydrothermal reaction between $Fe(C_2O_2)\cdot 2H_2O$, molybic acid, and ethylenediamine. The structure of 1 consists of 2-D layers formed by $[Fe(C_2O_4)MoO_4]^{2-}$ nets with $H_3N^+CH_2CH_2N^+H_3$ dications situated in the gaps. The structure of 2 features a double-layered structure formed by $FeMoO_4$ units that are capped by *cis*-coordinated $H_2NCH_2CH_2NH_2$ molecules.

INTRODUCTION

The widespread use of multiplex organic ligands for building novel coordination network compounds in recent years represents a paradigm shift in the design and synthesis of extended solid-state materials (1–7). Through judicious selection of metal ions and organic ligands, extremely complex but predictable structures can be constructed on the basis of certain coordination algorithms. In addition to their fascinating structures, such new materials may have useful sorptive, catalytic, magnetic, optical, or opto-electronic properties. On the other hand, inorganic oxides constitute an important class of materials whose applications span from heterogeneous catalysis to microelectronics and to superconductivity, to just name a few. Recently, there has been increasing interest in the synthesis of organic–inorganic hybrid oxide materials in the context of crystal engineering. This can not only broaden the horizon of structural chemistry, but also produce novel physical properties that are synergistic of the organic ligands and inorganic building blocks.

In light of their typical infinite open-framework structures with well-defined stoichiometries, the organic–inorganic hybrid oxide compounds present intriguing prospects of ordering organic chromophores for nonlinear optical (NLO) applications (8). We have been investigating the synthesis of such ordered supramolecular assemblies as molecule-based NLO materials using such methods as direct coordination of an organic chromophore to a metal center, lattice inclusion of chromophores in polymeric frameworks, and anion exchange with chromophores (9). In this paper, we present the synthesis and structural characterization of two novel organic–inorganic hybrid compounds, $(H_3NCH_2CH_2NH_3)[Fe(C_2O_4)MoO_4]$ (**1**) and $Fe(H_2NCH_2CH_2NH_2)$ MoO_4 (**2**), both resulting from our host–guest inclusion studies and consisting of 2-D structures derived from simple coordination building blocks.

EXPERIMENTAL

Chemicals in this work were purchased from either Aldrich or Strem and used as obtained. All manipulations were performed in air unless otherwise noted.

Synthesis and Characterization

$(H_3NCH_2CH_2NH_3)[Fe(C_2O_4)MoO_4]$ (**1**). A sample of 44 mg (0.30 mmol) of $Fe(C_2O_2)\cdot 2H_2O$, 100 mg (0.30 mmol) of molybic acid, and 33 mg (0.54 mmol) of ethylenediamine was sealed with 0.3 ml of H_2O in a thick-walled Pyrex tube. The reaction was carried out at 110°C for 24 hours to afford yellow single crystals of $(H_3NCH_2CH_2NH_3)[Fe(C_2O_4)$ $MoO_4]$ in ~75% yield. Analytically pure crystals were obtained by acetone and ether washing.

$Fe(H_2NCH_2CH_2NH_2)MoO_4$ (**2**). The red crystals of **2** were prepared in a way similar **1** using 100 mg (1.62 mmol) of ethylenediamine in the sealed tube. A small amount of **1** ($< 2\%$) was also formed after 24-hour heating of the tube. The different crystals of **1** (yellow tetragonal prisms) and **2**

[1] To whom correspondence should be addressed. Fax: 330-672-3816. E-mail: shuang1@kent.edu.

0022-4596/00 $35.00

TABLE 1
Crystal Data and Structure Refinement Results for 1 and 2

Compound	**1**	**2**
Empirical formula	$C_4H_{10}N_2O_8FeMo$	$C_2H_8N_2O_4FeMo$
Formula weight	365.92	275.88
Color/shape	Yellow/rectangular prism	red/platelet
Crystal system	Monoclinic	Monoclinic
Space group	$P2_1/c$ (No. 14)	$P2_1/c$ (No. 14)
Unit cell dimensions	$a = 5.5813(4)$ Å	$a = 10.433(1)$ Å
	$b = 13.994(1)$ Å	$b = 9.817(1)$ Å
	c = 13.2282(9) Å	$c = 7.1797(9)$ Å
	$\beta = 93.100(1)^\circ$	$\beta = 105.279(2)^\circ$
Volume	1031.7(1) Å^3	709.4(1) Å^3
Z	4	4
Density (calculated)	2.36 mg/m^3	2.58 mg/m^3
Absorption coefficient	2.649 mm^{-1}	3.766 mm^{-1}
$F(000)$	720.00	536.00
Crystal size	$0.22 \times 0.10 \times 0.06$ mm	$0.06 \times 0.04 \times 0.02$ mm
θ range for data collection	1.46 to 27.08°	2.03 to 26.95°
Reflections collected	5490	3676
Independent/observed refl.	2123/1681	1672/730
Absorption correction	SADABS	SADABS
Range of relat. transm. factors	1.00, 0.930	1.00, 0.871
Final R indices	$R = 0.0185/R_w = 0.0261$ $[I > 2.5\sigma(I)]$	$R = 0.0548/R_w = 0.0657$ $[I > 3.0\sigma(I)]$
Goodness-of-fit on F	0.99	0.95
Weighting scheme	$w = 1/[\sigma^2(F_o) + 0.00034\lvert F_o\rvert^2]$	$w = 1/[\sigma^2(F_o) + 0.00207\lvert F_o\rvert^2]$
Largest diff. peak and hole	0.40/ − 0.59 e Å^{-3}	2.14/ − 1.41 e Å^{-3}

(red platelets) can be readily separated by hand. The estimated yield for **2** is ~57%.

The phase identity and homogeneity of **1** and **2** were confirmed by comparing the experimental X-ray powder diffraction patterns of the bulk material with those calculated from the single-crystal X-ray data.

X-Ray Data Collection, Structure Solution, and Refinement

A proper crystal of **1** or **2** was selected from the reaction product and mounted on a thin glass fiber using epoxy cement. All measurements were made on a Bruker SMART CCD diffractometer with graphite-monochromated Mo$K\alpha$ radiation ($\lambda = 0.71069$ Å) operating at 50 kV and 40 mA.

The data were collected at 25°C using a narrow frame method with scan widths of 0.3° in ω and exposure times of 10 seconds. A hemisphere of intensity data was collected in 1081 frames with a crystal-to-detector distance of 50.4 mm, which corresponds to a maximum 2θ value of 54.1°. Frames were integrated with the SAINT program (10). A semi-empirical absorption correction based upon SADABS was applied to each data set.

Both structures were solved by direct methods and expanded using Fourier techniques. The nonhydrogen atoms were refined anisotropically. All the hydrogen atoms were directly located from electron density maps and included in the structures, but not refined. The maximum and minimum peaks on the final difference Fourier map corresponded to 0.40 and − 0.59 e$^-$/Å^3 for **1**, and 2.14 and − 1.41 e$^-$/Å^3 for **2**, respectively. In the structure of **2**, the positive peak is 0.94 Å from the Mo atom, and the negative peak is 0.96 Å from the same atom. Details of the data collection, structure solution, and refinement are given in Table 1.

RESULTS AND DISCUSSION

As part of our continuing search for infinite metal–organic coordination polymer hosts that can form inclusion compounds with organic NLO chromophores, we carried out a series of reactions between nitroanilines, $Fe(C_2O_2)\cdot 2H_2O$, molybic acid, and ethylenediamine (en). The rationale for such studies was to develop hybrid NLO materials that combine the attributes of inorganic, organic, polymeric, and crystalline materials. The possible advantages of this approach may be that (1) such organic–inorganic hybrid oxide hosts can possess robust, infinite crystalline structures with well-defined stoichiometries; (2) metal-to-ligand or ligand-to-metal charge transfer bands can potentially contribute to large second-order nonlinearities; and (3) covalently bonded hybrid metal oxides have higher thermal and chemical stability than most pure organic chromophore molecules. However, the subsequent structural investigations showed that none of these reactions gave inclusion compounds. Instead, they produced two novel organic–in-

TABLE 2
Atomic Coordinates and B_{eq} for 1

Atom	x	y	z	B_{eq}[a]
Mo	0.60703(4)	0.27382(1)	0.29233(1)	1.211(5)
Fe	0.51702(6)	0.02023(2)	0.24900(2)	1.144(7)
O1	0.4745(3)	0.3727(1)	0.2248(1)	1.74(4)
O2	0.9161(4)	0.2835(1)	0.2934(2)	2.37(4)
O3	0.5290(4)	0.2739(2)	0.4201(2)	2.57(5)
O4	0.5141(3)	0.1670(1)	0.2308(2)	2.13(4)
O5	0.8302(3)	0.0300(1)	0.3526(1)	1.57(3)
O6	0.8042(3)	0.0081(1)	0.1489(1)	1.60(4)
O7	1.2030(3)	0.0043(1)	0.1486(1)	1.50(3)
O8	1.2307(3)	0.0268(1)	0.3520(1)	1.69(4)
N1	1.1185(4)	0.1456(2)	− 0.0072(2)	2.19(5)
N2	1.2736(4)	0.3580(2)	0.0277(2)	1.98(5)
C1	1.0352(5)	0.2143(2)	0.0704(2)	1.92(5)
C2	1.0289(5)	0.3161(2)	0.0330(2)	2.26(6)
C3	1.0241(4)	0.0236(2)	0.3095(2)	1.19(5)
C4	1.0081(4)	0.0102(2)	0.1927(2)	1.13(4)

[a] $B_{eq} = 8/3\pi^2[U_{11}(aa^*)^2 + U_{22}(bb^*)^2 + U_{33}(cc^*)^2 + 2U_{12}(aa^*bb^*)\cos\gamma + 2U_{13}(aa^*cc^*)\cos + 2U_{23}(bb^*cc^*)\cos\alpha]$.

TABLE 3
Atomic Coordinates and B_{eq} for 2

Atom	x	y	z	B_{eq}[a]
Mo	0.3425(1)	0.3952(2)	0.2942(2)	1.37(3)
Fe	0.3797(2)	0.0307(2)	0.3140(3)	1.41(5)
O1	0.177(1)	0.365(1)	0.178(2)	2.6(3)
O2	0.354(1)	0.485(1)	0.513(1)	2.8(3)
O3	0.413(1)	0.490(1)	0.131(1)	1.4(2)
O4	0.424(1)	0.238(1)	0.348(1)	2.0(2)
N1	0.165(1)	0.052(1)	0.265(2)	2.2(3)
N2	0.326(1)	−0.183(1)	0.315(2)	2.1(3)
C1	0.109(2)	−0.078(2)	0.194(2)	1.8(4)
C2	0.187(2)	−0.194(2)	0.315(2)	2.0(4)

[a] $B_{eq} = 8/3\pi^2[U_{11}(aa^*)^2 + U_{22}(bb^*)^2 + U_{33}(cc^*)^2 + 2U_{12}(aa^*bb^*)\cos\gamma + 2U_{13}(aa^*cc^*)\cos + 2U_{23}(bb^*cc^*)\cos\alpha]$.

TABLE 5
Selected Bond Distances and Bond Angles for 2

Mo–O1	1.73(1)	Mo–O2	1.78(1)	Mo–O3	1.799(9)
Mo–O4	1.76(1)	Fe–O2	2.11(1)	Fe–O3	2.219(9)
Fe–O3*	2.13(1)	Fe–O4	2.08(1)	Fe–N1	2.19(1)
Fe–N2	2.17(1)	N1–C1	1.44(2)	N2–C2	1.46(2)
C1–C2	1.53(2)				

O1–Mo–O2	109.8(5)	O1–Mo–O3	107.5(5)
O1–Mo–O4	108.7(5)	O2–Mo–O3	112.2(5)
O2–Mo–O4	108.9(5)	O3–Mo–O4	109.8(5)
O2–Fe–O3	170.6(4)	O2–Fe–O3*	91.4(4)
O2–Fe–O4	98.7(4)	O2–Fe–N1	89.6(5)
O2–Fe–N2	88.4(5)	O3–Fe–O3*	85.1(4)
O3–Fe–O4	89.9(4)	N1–Fe–N2	80.9(5)

organic layered structures derived from the coordination building blocks.

The refined atomic coordinates and equivalent isotropic displacement parameters for **1** and **2** are reported in Tables 2 and 3, with selected bond distance and bond angle data in Tables 4 and 5. From its structure refinement, the asymmetric unit in **1** was shown to contain an $H_3N^+CH_2CH_2N^+H_3$ dication, an oxalate $C_2O_2^{2-}$ anion, an MoO_4^{2-} anion, and an iron atom. All the H atoms were directly located from the difference Fourier maps. The oxidation state of the iron can be unambiguously assigned as $2+$ on the basis of charge neutrality. All the atoms are situated on general positions. Figure 1 is the symmetry-expanded local structure for **1** that shows the atom connectivities and coordination environments. The Fe^{2+} ion is in a slightly distorted octahedral geometry with four equatorial O atoms from two neighboring oxalate anion and two axial O atoms from the bridging MoO_4^{2-} anion. The Fe–O bond distances range from 2.068(2) to 2.167(2) Å, and O–Fe–O bond angles involving the neighboring O atoms range from 86.97(7) to 91.73(8)°. The tetrahedral MoO_4^{2-} anion acts as a bridging ligand that connects two different Fe^{2+} centers. The bond distances of the Mo–O involving the doubly bridging O atoms are Mo–O1 = 1.786(2) and Mo–O4 = 1.766(2) Å, while the bond distances of the Mo–O involving the terminal O atoms are Mo–O2 = 1.730(2) and Mo–O3 = 1.768(2) Å, respectively. The expansion of this structural motif gives rise to one-dimensional $[Fe(C_2O_2)]_n$ chains connected by the MoO_4^{2-} groups. The overall structure of **1** can be described as two-dimensional $[Fe(C_2O_4)MoO_4]^{2-}$ layers with the $H_3N^+CH_2CH_2N^+H_3$ dications situated in the gaps. There are strong H bonds formed between the ammine groups of the ammonium cations and the MoO_4^{2-} and oxalate anions with the typical O ⋯ H distances from ca. 1.84 to 2.06 Å. Alternatively, the

TABLE 4
Selected Bond Distances and Bond Angles for 1

Mo–O1	1.786(2)	Mo–O2	1.730(2)	Mo–O3	1.768(2)
Mo–O4	1.766(2)	Fe–O1	2.093(2)	Fe–O4	2.068(2)
Fe–O5	2.167(2)	Fe–O6	2.140(2)	Fe–O7	2.153(2)
Fe–O8	2.158(2)				
O5–C3	1.253(3)	O6–C4	1.249(3)	O7–C4	1.265(3)
O8–C3	1.256(3)	N1–C1	1.499(4)	N2–C2	1.492(4)
C1–C2	1.507(4)	C3–C4	1.553(3)		

O1–Mo–O2	109.25(9)	O1–Mo–O3	111.16(9)
O1–Mo–O4	108.81(8)	O2–Mo–O3	106.8(1)
O2–Mo–O4	109.74(9)	O3–Mo–O4	111.1(1)
O1–Fe–O4	177.08(8)	O1–Fe–O5	86.97(7)
O1–Fe–O6	90.74(7)	O1–Fe–O7	90.58(7)
O1–Fe–O8	87.05(7)	O5–Fe–O6	77.90(6)
O5–Fe–O7	177.45(7)	O5–Fe–O8	101.40(6)

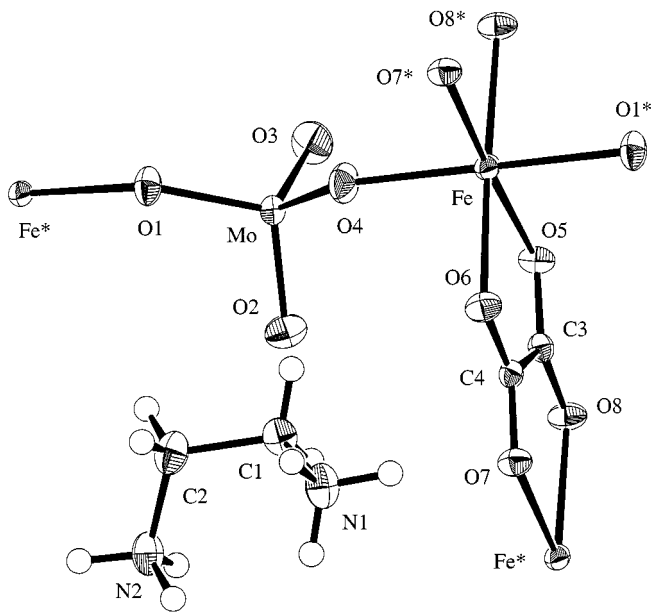

FIG. 1. ORTEP representation of the local structure in **1**, showing the atom connectivities and coordination environments.

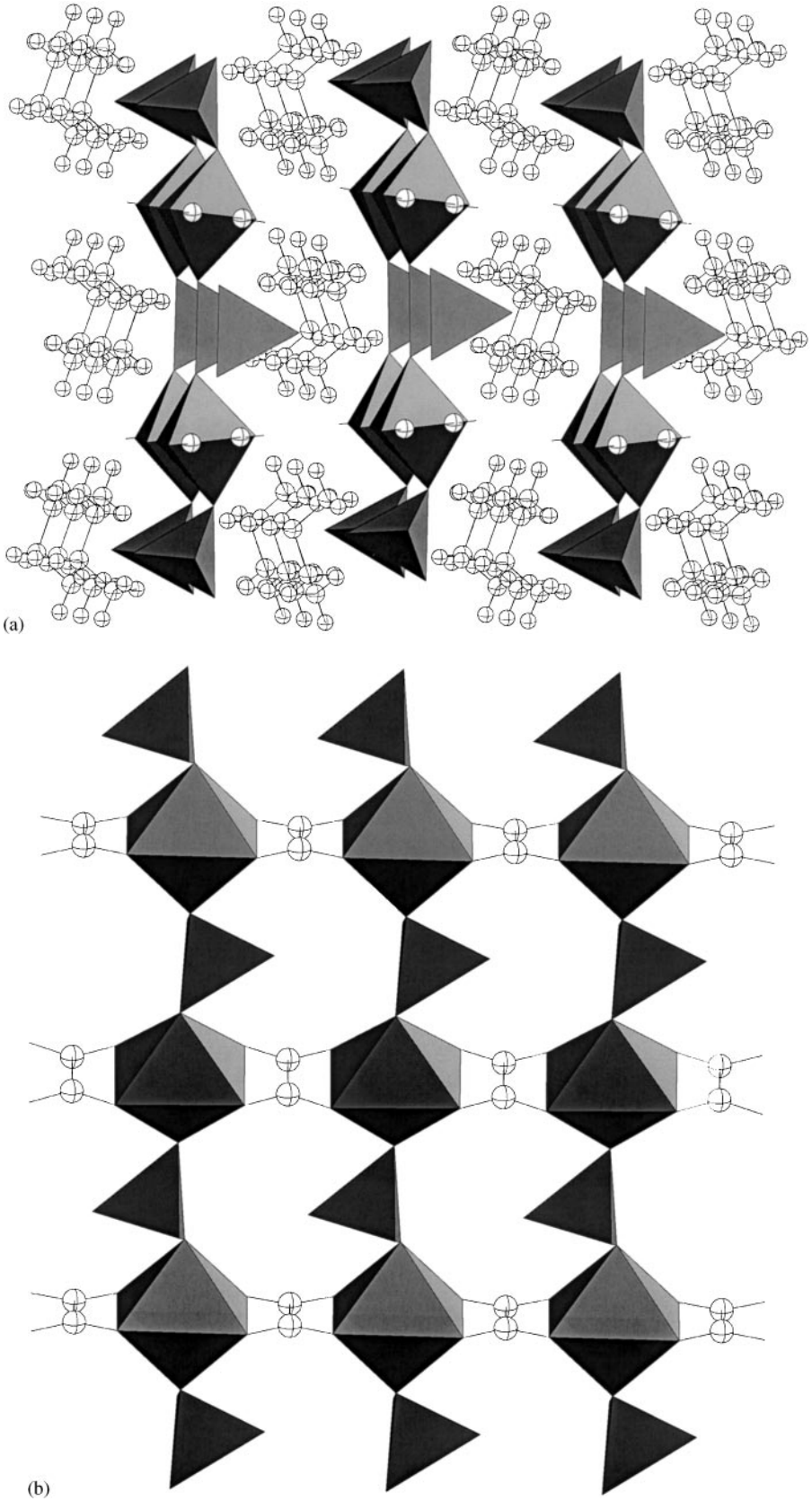

FIG. 2. Projections of **1** in (A) the *bc* plane and (B) the *ab* plane.

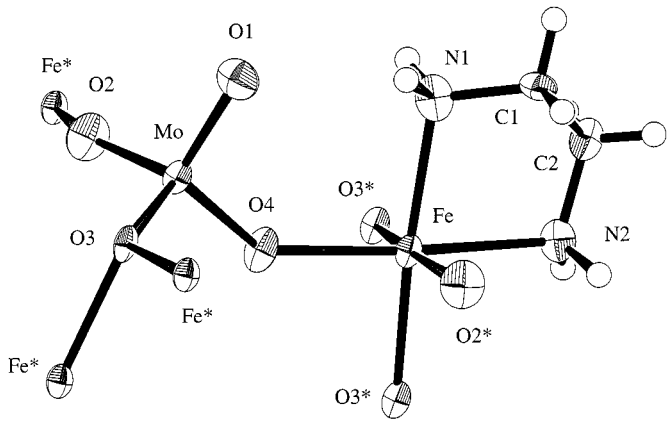

FIG. 3. ORTEP representation of the local structure in **2**, showing the atom connectivities and coordination environments.

2-D networks can be viewed as being formed by connecting the 1-D FeO_6 octahedral arrays with the MoO_4 tetrahedra through corner-sharing at the axial positions of the octahedra. It is interesting to note that the two terminal O atoms from the MoO_4^{2-} groups point to the same direction within two neighboring $[Fe(C_2O_2)]_n$ chains, but alternate from one array to another. The presence of a C–C unit in the oxalate anion prevents the FeO_8 octahedra from sharing their edges. Figure 2 shows two different polyhedron representations of **1** projected in the *bc* and *ab* planes with and without the cations. Similarly, all the atoms in the crystallographic unit cell of **2** are situated on general positions. The asymmetric unit contains a chelate $H_2NCH_2CH_2NH_2$ ligand, an Fe^{2+} ion, and a bridging MoO_4^{2-} anion. Figure 3 depicts the symmetry-expanded local structure for **2** that shows the atom connectivities and coordination environments. First, the Fe^{2+} ion is now in a more distorted octahedral environment involving two *cis* N atoms and four O atoms from the MoO_4^{2-} anion. The Fe–O and Fe–N bonds average 2.13(1) and 2.18(1) Å, respectively. The O–Fe–O bond angles involving the neighboring O or N atoms range from 83.2(4) to 98.7(4)°. The MoO_4^{2-} anion contains a triply bridging atom, two doubly bridging atoms, and a terminal O atom. The symmetry expansion showed that **2** can best be described as a double-layer structure with $FeMoO_4$ units forming two fused layers that are capped by *cis*-coordinated $H_2NCH_2CH_2NH_2$ molecules as shown in Fig. 4. More specifically, the double layer consists of edge-shared FeN_2O_4 octahedra connected by the MoO_4 tetrahedra through corner-sharing. Figure 5 shows two different projections of the structure with the C atoms in $H_2NCH_2CH_2NH_2$ ligand omitted for clarity.

In conclusion, we have synthesized and structurally characterized two novel organic–inorganic layered compounds. The formation of **1** and **2** attests to the diverse structural chemistry of this and similar organic–inorganic hybrid systems. In light of their synthetic simplicity, such systems are well-suited for exploratory investigations of novel or useful chemical and physical properties.

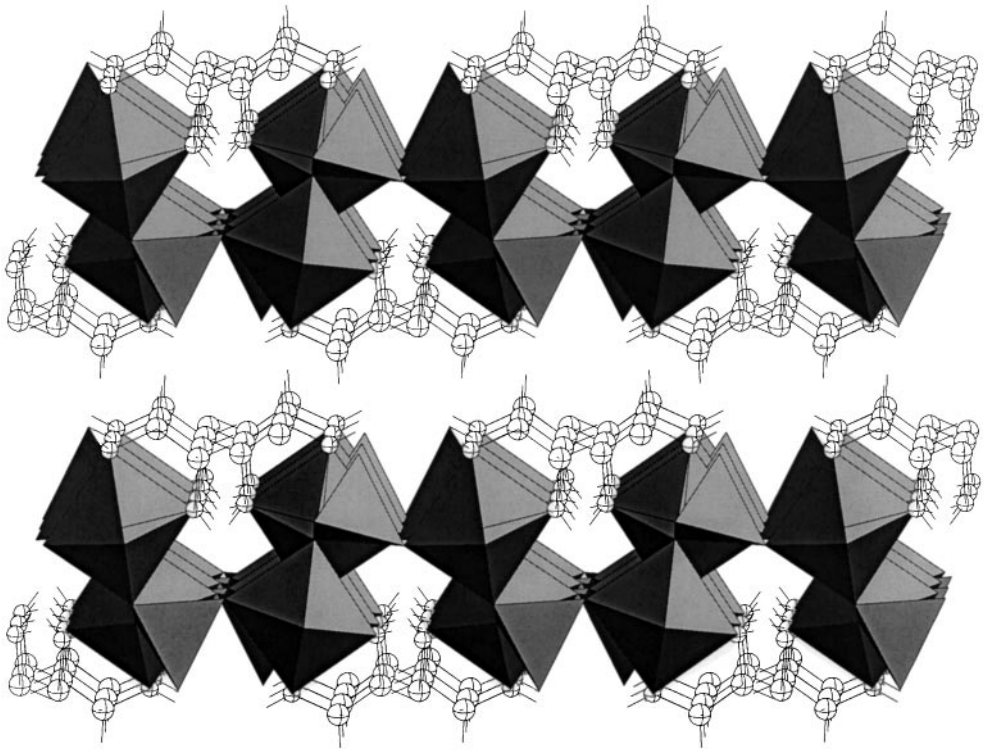

FIG. 4. Polyhedron representation of structure **2**.

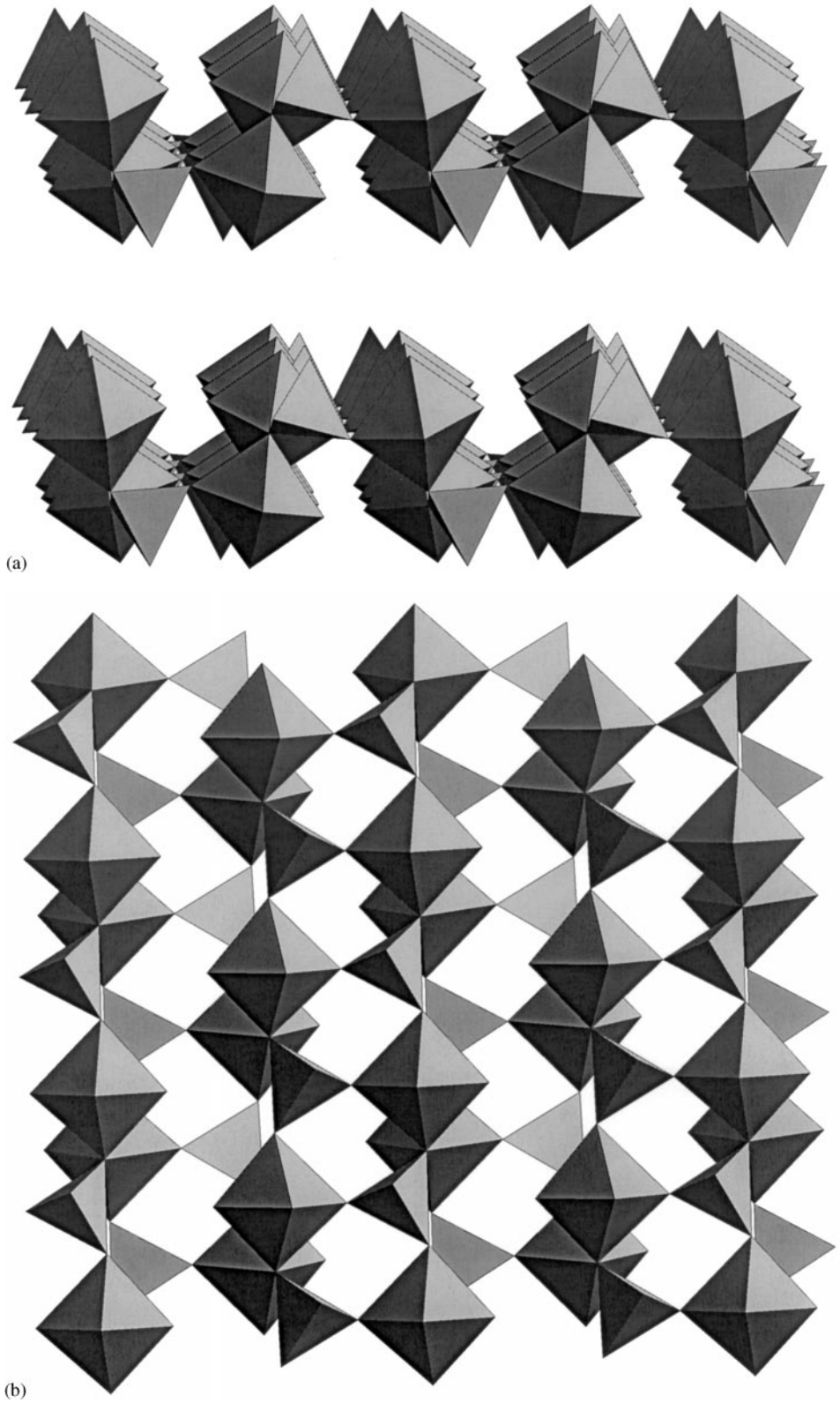

FIG. 5. Projections of **2** in (A) the *ab* plane and (B) the *bc* plane.

ACKNOWLEDGMENTS

We thank Kent State University for the startup funds provided for the initial study of this project. S.D.H. is a recipient of the NSF CAREER award for 1998–2002 (DMR-9996287).

REFERENCES

1. (a) R. W. Gable, B. F. Hoskins, and R. Robson, *J. Chem. Soc., Chem. Commun.* 1677 (1990); (b) B. F. Abrahams, B. F. Hoskins, and R. Robson, *J. Am. Chem. Soc.* **113,** 3603 (1991); (c) R. Robson, B. F. Abrahams, S. R. Batten, R. W. Gable, B. F. Hoskins, and J. Liu, "Supramolecular Architecture." Am. Chem. Soc. Washington, DC, 1992.
2. (a) M. Fujita, Y. J. Kwon, S. Washizu, and K. Ogura, *J. Am. Chem. Soc.* **116,** 1151 (1994); (b) M. Fujita, Y. J. Kwon, O. Sasaki, K. Yamaguchi, and K. Ogura, *J. Am. Chem. Soc.* **117,** 7287 (1995).
3. (a) O. M. Yaghi and H. Li, *J. Am. Chem. Soc.* **117,** 10401 (1995); (b) O. M. Yaghi and G. Li, *Angew. Chem., Int. Ed. Engl.* **34,** 207 (1995); (c) O. M. Yaghi, G. M. Li, and H. L. Li, *Nature* **378,** 703 (1995).
4. (a) L. R. MacGillivray, S. Subramanian, and M. J. Zaworotko, *J. Chem. Soc., Chem. Commun.* 1325 (1994); (b) M. J. Zaworotko, *Chem. Soc. Rev.* **23,** 284 (1994); (c) S. Subramanian and M. J. Zaworotko, *Angew. Chem., Int. Ed. Engl.* **34,** 2127 (1995).
5. (a) L. Carlucci, G. Ciani, D. M. Proserpio, and A. Sironi, *J. Am. Chem. Soc.* **117,** 4562 (1995); (b) L. Carlucci, G. Ciani, D. M. Proserpio, and A. Sironi, *J. Chem. Soc., Chem. Commun.* 2755 (1994).
6. (a) D. Venkataraman, G. B. Gardner. S. Lee, and J. S. Moore, *J. Am. Chem. Soc.* **117,** 11600 (1995); (b) D. Venkataraman, S. Lee, J. Zhang, and J. S. Moore, *Nature* **371,** 591 (1994).
7. (a) Y. P. Zhang, J. R. D. DeBord, C. J. O'Conner, R. C. Haushalter, A. Clearfield, and J. Zubieta, *Angew. Chem., Int. Ed. Engl.* **35,** 989 (1996); (b) D. Hagrman, C. Zubieta, J. Zubieta, and R. C. Haushalter, *Angew. Chem., Int. Ed. Engl.* **36,** 873 (1997); (c) D. Hagrman and J. Zubieta, *Chem. Commun.* 2005 (1998).
8. For recent reviews, see (a) T. J. Marks and M. A. Ratner, *Angew. Chem., Int. Ed. Engl.* **34,** 155 (1995); (b) N. J. Long, *Angew. Chem., Int. Ed. Engl.* **34,** 21 (1995); (c) L. R. Dalton, A. W. Harper, R. Ghosn, W. H. Steir, M. Ziari, H. Fetterman, Y. Shi, R. V. Mustacich, A. K.-Y. Jen, and K. J. Shea, *Chem. Mater.* **7,** 1060 (1995).
9. (a) S. D. Huang and R.-G. Xiong, *Polyhedron* **16,** 3929 (1997); (b) S. D. Huang, R.-G. Xiong, J. Han, and B. R. Weiner, *Inorg. Chim. Acta* **294,** 95 (1999); (c) B. Liu and S. D. Huang, work in progress.
10. Bruker Analytical X-ray Systems, Inc. SAINT program version 4, 1994–1996; 6300 Enterprise Lane, Madison, WI 53719.